Band structures in ^{106}Ag and systematics of shears mechanism in the $A \sim 110$ mass region

C. Y. He (贺创业),[1,*] L. H. Zhu (竺礼华),[1,2] X. G. Wu (吴晓光),[1] S. X. Wen (温书贤),[1] G. S. Li (李广生),[1] Y. Liu (刘颖),[1] Z. M. Wang (王治民),[1] X. Q. Li (李雪琴),[1] X. Z. Cui (崔兴柱),[3] H. B. Sun (孙慧斌),[2] R. G. Ma (马瑞刚),[1] and C. X. Yang (杨春祥)[1]

[1]*China Institute of Atomic Energy, Beijing 102413, China*

[2]*School of Science, Shenzhen University, Shenzhen 518060, China*

[3]*Department of Physics, Jilin University, Changchun 130023, China*

(Received 9 February 2010; published 14 May 2010)

High-spin states of ^{106}Ag were populated via the fusion-evaporation reaction ^{100}Mo (^{11}B,5n)^{106}Ag at a beam energy of 60 MeV. A rich level scheme with six band structures has been established. A high-K negative-parity band has been identified and assigned to the $\pi g_{9/2} \otimes \nu[h_{11/2}(g_{7/2}/d_{5/2})^2]$ configuration. The positive parity $\triangle I = 1$ band, built on the 12^+ state, is discussed in terms of the magnetic rotation model. The systematic study of similar bands in the $A \sim 110$ mass region indicates that the magnetic rotation phenomenon has, as lower boundary, the Ag isotopes at $Z = 47$.

DOI: 10.1103/PhysRevC.81.057301 PACS number(s): 21.10.Re, 23.20.Lv, 27.60.+j

The spectroscopic study of nuclei in the $A \sim 110$ mass region with $Z \sim 50$ has provided a wealth of information on different nuclear symmetries, giving rise to so-called magnetic bands [1–5] and chiral bands [6–9] as well as a rich variety of collective behavior. In this region, neutrons fill successively the $d_{5/2}$, $g_{7/2}$, and high-j $h_{11/2}$-intruder orbitals, while proton holes occupy the high-j $g_{9/2}$ orbital. So far, several sequences of magnetic dipole transitions very much resembling the character of a collective rotational band have been established in the nuclei around $Z \sim 50$. These bands are also called shears bands since here the total angular momentum is generated, in the framework of the tilted axis cranking (TAC) model, through the shears mechanism [10]. Chiral bands have also been proposed in several $Z = 45$ isotopes of this region, suggesting a small island of chiral rotation centered around ^{104}Rh. The $Z = 47$ nucleus ^{106}Ag, with two more protons with respect to ^{104}Rh, is just between the island of chirality and the region where magnetic dipole bands have been identified in the mass $A \sim 110$ region. In this respect, ^{106}Ag could be an interesting case where both shears bands and chiral bands can coexist. In this Brief Report, we report new detailed experimental information on ^{106}Ag.

High-spin states in ^{106}Ag were populated through the ^{11}B + ^{100}Mo reaction. The target consisted of a 2.5 mg/cm^2 foil of ^{100}Mo (isotopically enriched to 97.4%) on a 11 mg/cm^2 lead backing. The ^{11}B beam was delivered by the HI-13 tandem accelerator of the China Institute of Atomic Energy. To determine the optimum beam energy for producing ^{106}Ag, γ-ray excitation functions were measured at beam energies of 52, 56, 60, and 64 MeV; the beam energy of 60 MeV was then chosen for the γ-γ coincidence measurement. An array consisting of 14 Compton-suppressed HPGe detectors was used to collect γ-γ coincidence data. The Ge detectors in the array were placed, with respect to the beam direction, as follows: four at 90°, five at about 48°, and five at about 132°. Each detector had an energy resolution of about 2 keV for 1332.5 keV γ rays. Energy and efficiency calibration of the detectors was performed using standard sources such as ^{60}Co and ^{152}Eu. To avoid the presence of the K-x rays of lead in the γ spectra, a lower limit of 90 keV was set in the electronic system. Events have been collected, in an event-by-event mode, when at least two Compton-suppressed Ge detectors fired in coincidence. A total of 130×10^6 γ-γ coincidence events were recorded. The data were sorted into a fully symmetrized E_γ-E_γ coincidence matrix as well as into an asymmetric directional correlation ratios of oriented states (DCO) matrix. These matrices were analyzed with the RADWARE program [11]. The DCO matrix was created by sorting on one axis the detectors placed at ∼48° and ∼132° with respect to the beam direction and on the other axis those at ∼90°. In our array geometry, if one gates on a stretched quadrupole transition, the expected DCO ratios are close to 1.0 for stretched quadrupole transitions and around 0.6 for pure dipole transitions. Spin and parity assignments of excited states were based, where possible, on the DCO ratios measured for the deexciting γ transitions.

The level scheme of the ^{106}Ag nucleus deduced from the present study is shown in Fig. 1. High-spin states of ^{106}Ag have been studied previously by Popli *et al.* [12] and Jerrestam *et al.* [13]. We confirm the major part of the ^{106}Ag level scheme known from previous studies. In the following, we illustrate what has been modified or extended in the level scheme: (a) positive parity states, whereby new γ-ray transitions with energies of 491, 642, 554, and 295 keV have been placed at the bottom of band 1; the band is also extended at higher energy with the new transitions of 585, 628, 1173, and 1213 keV, and another transition connecting band 1 to band 6 was observed with an energy of 243 keV; and (b) negative parity states, whereby band 2 of our level scheme comprises all the transitions assigned to the band labeled 5 in Ref. [13], apart from the 625 keV transition discussed in this reference; in addition, four new crossover $E2$ transitions have been observed, thereby reordering the dipole transitions above $14\hbar$. The DCO ratios measured for the 506 and 510 keV transitions linking band 2 to band 3 are both in agreement

*chuangye.he@gmail.com

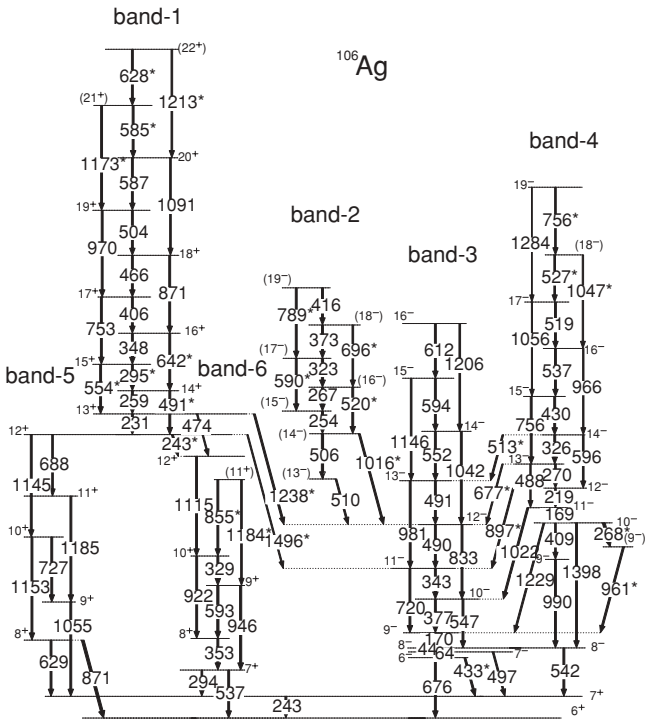

FIG. 1. Level scheme of ^{106}Ag resulting from the present work. It is built on the 6^+ β-decaying isomer at 89 keV. Energies are in keV. New γ transitions are indicated by asterisks.

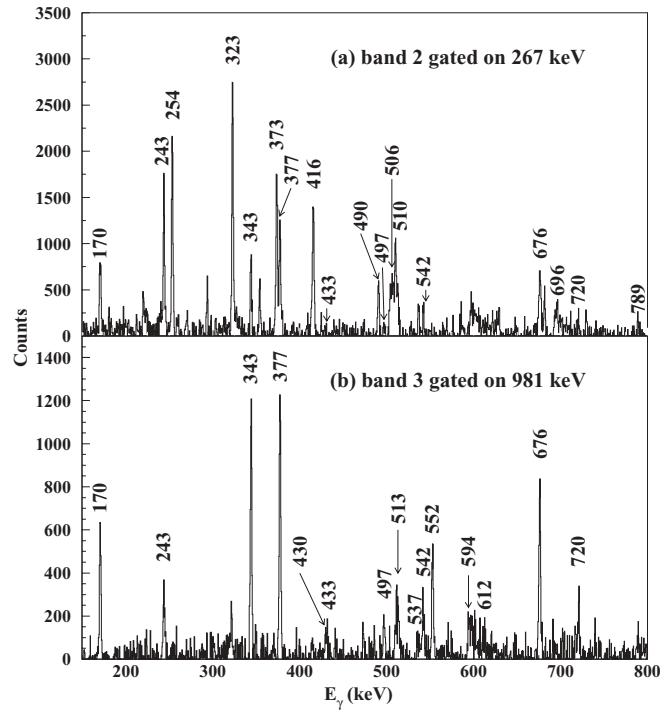

FIG. 2. Selected coincidence spectra for bands (a) 2 and (b) 3 in ^{106}Ag.

with a $\Delta I = 1$ assignment (as in Ref. [13]). Furthermore, the observation of the 1016 keV crossover transition favors strongly a negative parity for the states of this band, as shown in Fig. 1. The 510 keV transition feeds the 12^- state of band 3, whereas in the earlier study [13], it was feeding the 9^- state of the same band. In fact, in our work, all the transitions of band 2 as well as the transitions linking bands 2 and 3 were found to be in coincidence with all the transitions below the 12^- of band 3 but not with the transitions above. Band 2 is therefore built, at variance with Ref. [13], above the 12^- level of band 3, as one can see in Fig. 1. The γ-ray spectra shown in Fig. 2, the upper one in coincidence with the 267 keV transition of band 2 and the lower one with the 981 keV transition of band 3, support this conclusion. Because of the 90 keV threshold of our electronics, we coud not observe the 44 and 64 keV transitions of band 3 that are placed in the level scheme following Ref. [13]. Finally, (c) we have also identified for the first time two transitions, of 1238 and 1496 keV, linking the negative and positive parity structures of ^{106}Ag. Preliminary results on the level scheme derived from this work have been published in Ref. [14]. In the following, we will concentrate the discussion on bands 1 and 2 in the framework of the magnetic rotation phenomenon in the $A \sim 110$ mass region.

As discussed earlier, the major difference between the level scheme proposed in Fig. 1 and the one of Ref. [13], apart from the extension to higher spins of bands 1 and 5, is the placement of band 2 (band 5 in Ref. [13]) at a higher excitation energy and spin together with some reordering of its levels. The level spacings of band 2 appear now to be of rotational character, even if not those of a well-deformed rotor. The observed strong $M1$ and weak $E2$ crossover transitions [see the spectrum gated by the 267 keV transition in Fig. 2(a)] denote a large magnetic moment for this band. Several studies (e.g., Refs. [15,16]) showed that the coupling between deformation-aligned quasiprotons and rotation-aligned quasineutrons, or vice versa, can greatly enhance the magnetic moment and increase the reduced $M1$ transition probability. Considering the proton and neutron numbers in ^{106}Ag, the configuration of band 2 is probably based on valence protons occupying the upper substates of the $g_{9/2}$ orbital and on valence neutrons lying in the lower substates of the $h_{11/2}$ orbital. Band 2 decays only into band 3 with the same negative parity. The angular momentum as a function of rotational frequency ω, that for shears bands, is defined as $\hbar\omega(I) = E(I) - E(I-1)$ and is plotted in Fig. 3. The aligned angular momentum of band

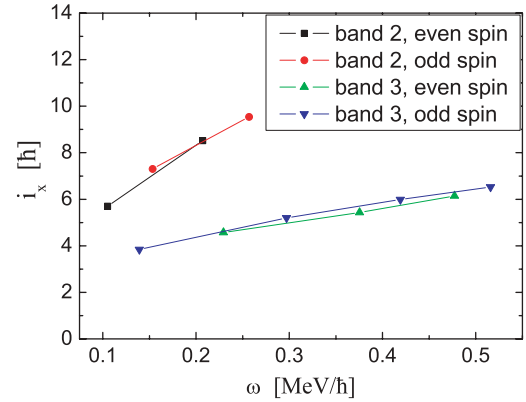

FIG. 3. (Color online) Experimental aligned spin as a function of rotational frequency ω for bands 2 and 3 in ^{106}Ag.

2 is from 3 to 5$\hbar$ higher than that of band 3, in which the Harris parameters used for reference, taken from Ref. [14], are $J_0 = 8.9\hbar^2$ MeV^{-1} and $J_1 = 15.7\hbar^4$ MeV^{-3}. The gain in alignment of band 2 with respect to band 3 is expected from the alignment of a pair of $g_{7/2}$ or $d_{5/2}$ neutrons. On the basis of the configuration previously assigned to band 3, $\pi g_{9/2} \otimes \nu h_{11/2}$ [12], the configuration of band 2 is most probably $\pi g_{9/2} \otimes \nu[h_{11/2}(g_{7/2}/d_{5/2})^2]$. High-$K$ bands of similar character have already been observed in this region, for example, in the ^{108}In isotone [3] and in the neighboring odd-odd nucleus ^{110}In [3]. This supports the configuration assignment given to band 2 of ^{106}Ag.

The positive-parity $\Delta I = 1$ band 1, built on top of bands 5 and 6, has been interpreted as a magnetic rotational band based on the $\pi g_{9/2} \otimes \nu[h^2_{11/2}(g_{7/2}/d_{5/2})]$ configuration [17,18]. A band crossing at $\hbar\omega \sim 0.59$ MeV was explained by the alignment of a $\nu d_{5/2}$ or $\nu g_{7/2}$ pair [17], and then this band was observed to 22$\hbar$. To better understand the character of band 1, the experimental data have been compared with TAC [19] calculations [15], assuming the configuration given earlier. The angular momentum as a function of rotational frequency ω is plotted in Fig. 4. The present experimental results are in better agreement with the calculations than the previous data. This comparison with the TAC calculations confirms that the total angular momentum of the band can be mainly explained through the shears mechanism.

Bands 1 and 2 appear to have very similar character, both of them showing a high-K $\Delta I = 1$ rotational structure. Their apparent similar rotational characters can be explained through two different mechanisms. Band 2 has been extended up to spin 19, but the angular momentum from valence particles can only increase by 2 units from the 14$\hbar$ band head. This suggests that in addition to the shears mechanism, the collective rotation around a principal axis contributes. Several bands with this character have been found in this mass region, as the bands with $\pi g_{9/2} \otimes \nu h^2_{11/2}$ and $\pi g_{9/2} \otimes \nu[h_{11/2}(g_{7/2}/d_{5/2})]$ configurations in the ^{105}Ag [20] and ^{107}Ag isotopes [13,21], respectively. Collective rotation around the principal axis contributes only marginally to the angular momentum of the band head, but such contribution grows quickly with spin.

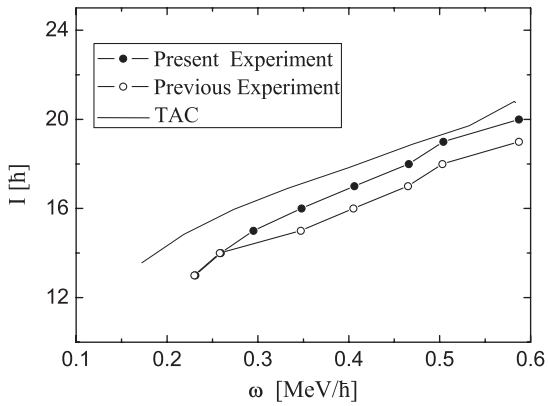

FIG. 4. Angular momentum as a function of rotational frequency for band 1 of ^{106}Ag. The filled and open circles refer to the present and previous experimental results [13], respectively. For comparison, calculations using the TAC model are shown with a solid line.

On the other side, the major part of the total angular momentum in band 1 is originated by the coupling of valence protons and neutrons through the shears mechanism. Structures with the same configuration as band 1 were also reported in this mass region, as, for example, in the odd-odd nuclei ^{104}Ag [22], ^{108}In [3], ^{110}In [3], ^{112}In [23], and ^{102}Rh [24]. They were interpreted as magnetic rotational bands in ^{104}Ag and ^{108,110,112}In. In Ref. [25], where the spectroscopic study of the ^{108}Ag nucleus was presented, the level structure and deexcitation mode of band 6 built on the $12^+\hbar$ state are very similar to band 1 in ^{106}Ag. The maximum angular momentum of band 6 in ^{108}Ag is 17$\hbar$, which is consistent with the maximum angular momentum provided by the $\pi g_{9/2} \otimes \nu[h^2_{11/2}(g_{7/2}/d_{5/2})]$ configuration. Band 6 in ^{108}Ag is therefore most probably another good case of a magnetic rotational band. Shears bands and collective bands can be characterized by the large difference in their $J^{(2)}/B(E2)$ ratios: It is $\sim 100\hbar^2$ MeV^{-1} (eb)$^{-2}$ for shears bands, while for a well-deformed nucleus, it is $\sim 10\hbar^2$ MeV^{-1} (eb)$^{-2}$. Lifetimes are available for some states in ^{105,106}Ag [15] but not for the high spin levels. Anyway, the derived $J^{(2)}/B(E2)$ ratios for the low-spin states of the bands in ^{105}Ag and the shears band in ^{106}Ag are not very different. It is therefore assumed that the gradual alignment of quasiparticles plays a major role, and that contribution from collective rotation at the band beginning in ^{105}Ag is very small. The TAC calculations of Ref. [19] have confirmed this interpretation.

We have calculated the dynamical moment of inertia $J^{(2)}$ for the positive-parity $\Delta I = 1$ bands discussed earlier in ^{104,106,108}Ag, ^{108,110,112}In, and ^{102}Rh and compared it with the $J^{(2)}$ of the normal deformed band in ^{130}Ba [26] and with the superdeformed band in ^{152}Dy [27] (see Fig. 5). The moment of inertia J for a rigid-spherical rotor at normal deformation depends on the mass A of the nucleus, $J \simeq A^{5/3}/72$. To remove the mass dependence, $72J^{(2)}/A^{5/3}$ is plotted as a function of rotational frequency ω in Fig. 5. One can clearly observe that such a quantity is almost constant at around 0.9 for ^{130}Ba and at the higher value of 1.5 for ^{152}Dy. However,

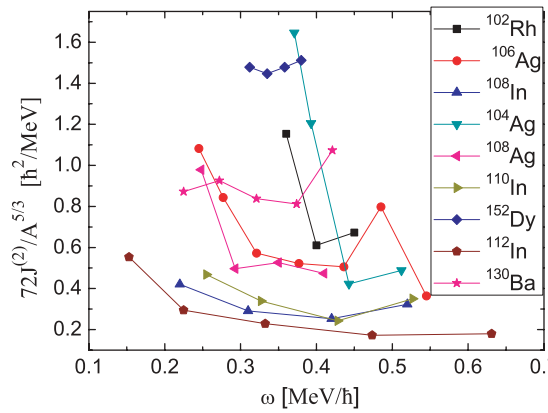

FIG. 5. (Color online) Dynamic momentum of inertia [$J^{(2)}$] as a function of rotational frequency (ω) for positive parity $\Delta I = 1$ bands in ^{104,106,108}Ag, ^{108,110}In, and ^{102}Rh. For comparison, the moment of inertia is plotted also for the normal-deformed rotational band of ^{130}Ba and and for the superdeformed band of ^{152}Dy.

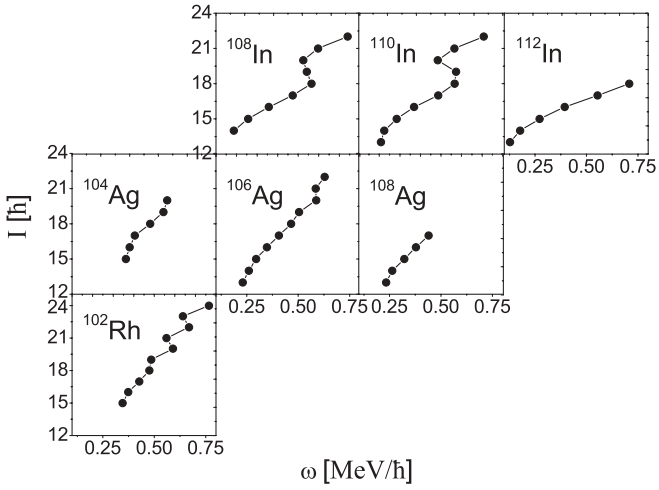

FIG. 6. Angular momentum as a function of rotational frequency (ω) for positive parity $\Delta I = 1$ bands in ^{104,106,108}Ag, ^{108,110}In, and ^{102}Rh.

most of the values for band 1 of ^{106}Ag are lower, at around 0.6; they are much smaller along the whole bands in ^{108,110,112}In. This is a strong indication that their structures of both Ag and In isotopic nuclei listed in Fig. 5 are mainly due to the shears mechanism coupling mode and not to the collective rotation of a deformed nucleus. One may notice also that with decreasing mass number A, the $72J^{(2)}/A^{5/3}$ values approach those of a normal deformed band; the nucleus ^{102}Rh, having the lowest mass number of those nuclei considered, has the value closest to ^{130}Ba. This can be explained by the fact that the $Z = 45$ nucleus ^{102}Rh, being far away from the $Z = 50$ closed shell, has more collective properties than the Ag and In isotopes.

The spins I of the positive parity band 1 in ^{106}Ag as well as the corresponding bands in In and Rh isotopes are plotted as a function of ω in Fig. 6. One can note the staggering at high spin of the $M1$ transition energies in ^{102}Rh, which is absent in the Ag and In isotopes. The staggering is usually associated with signature splitting, which can be defined by the expression $\triangle E = E(I) - E(I-1)$, where E and I are the energy and angular momentum of the state of interest, respectively. Signature splitting is a well-established phenomenon for collective rotations in well-deformed nuclei and cannot be associated with magnetic rotation. Since the deformation in ^{102}Rh is larger, the collective angular momentum grows much more quickly as a function of rotational frequency than in the In and Ag isotopes. As a consequence, the higher spin states are increasingly dominated by the collective angular momentum because of rotation, and the characteristics of a magnetic rotation band built through the shears mechanism disappear. The results shown in Figs. 5 and 6 seem therefore to indicate that the presence of magnetic rotational bands in the $A \sim 110$ mass region has a lower limit at $Z = 47$ in the Ag isotopes. However, to really prove this conclusion, more data are necessary for Rh nuclei to check if shears bands exist, for example, in ^{104}Rh, the isotone of ^{106}Ag.

In conclusion, a detailed level scheme for the ^{106}Ag nucleus has been built from our γ-ray spectroscopy study. The negative parity band 2 has been discovered and assigned to the $\pi g_{9/2} \otimes \nu[h_{11/2}(g_{7/2}/d_{5/2})^2]$ configuration. The magnetic rotational behavior of band 1 has been discussed and compared with that of similar bands of the $A \sim 110$ mass region. From the data available up to now, it seems that a lower Z limit for the presence of magnetic rotation in the $A \sim 110$ mass region is reached in the Ag isotopes with $Z = 47$.

The authors would thank to the crew of the HI-13 tandem accelerator in the China Institute of Atomic Energy for steady operation of the accelerator and for preparing the target. Manuscript correction and valuable suggestions for the physical discussion from Professor Santo Lunardi, who is working at Padova University (Italy), are also gratefully acknowledged. This work is partially supported by the National Natural Science Foundation of China under Contract No. 10375092, 10575133, 10675171, and 10775184 and by the Chinese Major State Basic Research Development Program through Grant No. 2007CB815005.

[1] N. S. Kelsall *et al.*, Phys. Rev. C **61**, 011301(R) (1999).
[2] C. J. Chiara *et al.*, Phys. Rev. C **61**, 034318 (2000).
[3] C. J. Chiara *et al.*, Phys. Rev. C **64**, 054314 (2001).
[4] D. G. Jenkins *et al.*, Phys. Lett. B **428**, 23 (1998).
[5] D. G. Jenkins *et al.*, Phys. Rev. Lett. **83**, 500 (1999).
[6] C. Vaman *et al.*, Phys. Rev. Lett. **92**, 032501 (2004).
[7] J. Timár *et al.*, Phys. Rev. C **73**, 011301(R) (2006).
[8] J. Timár *et al.*, Phys. Lett. B **598**, 178 (2004).
[9] P. Joshi *et al.*, Phys. Lett. B **595**, 135 (2004).
[10] S. Frauendorf *et al.*, Nucl. Phys. A **617**, 131 (1997); Rev. Mod. Phys. **73**, 463 (2001).
[11] D. C. Radford, Nucl. Instrum. Methods **361**, 297 (1995).
[12] R. Popli, F. A. Rickey, L. E. Samuelson, and P. C. Simms, Phys. Rev. C **23**, 1085 (1981).
[13] D. Jerrestam *et al.*, Nucl. Phys. A **577**, 786 (1994).
[14] C. Y. He *et al.*, High Energy Phys. Nucl. Phys. **30**, 966 (2006) (in Chinese).
[15] J. Tréherne *et al.*, Phys. Rev. C **27**, 166 (1983).
[16] A. I. Levon *et al.*, Z. Phys. A **343**, 131 (1992).
[17] C. Y. He *et al.*, Chin. Phys. C **32(II)**, 120 (2008).
[18] A. Y. Deo *et al.*, Phys. Rev. C **73**, 034313 (2006).
[19] V. I. Dimitrov, F. Donau, and S. Frauendorf, Phys. Rev. C **62**, 024315 (2000).
[20] J. Timár *et al.*, Phys. Rev. C **76**, 024307 (2007).
[21] F. R. Espinoza-Quinones *et al.*, Phys. Rev. C **55**, 1548 (1997).
[22] P. Datta *et al.*, Phys. Rev. C **69**, 044317 (2004).
[23] C. Y. He *et al.*, Nucl. Phys. A **834**, 84 (2010).
[24] J. Gizon *et al.*, Phys. Rev. C **59**, R570 (1999).
[25] F. R. Espinoza-Quinones *et al.*, Phys. Rev. C **52**, 104 (1995).
[26] O. Stuch *et al.*, Phys. Rev. C **61**, 044325 (2000).
[27] T. Lauritsen *et al.*, Phys. Rev. Lett. **88**, 042501 (2002).